

Photophysical, Electrochemical and Photovoltaic Properties of Porphyrin-Based Dye Sensitized Solar Cell

William Ghann¹, Tulio Chavez-Gil^{2*}, Carentxa I. Goede², Hyeonggon Kang¹, Shamsuddin Khan¹, Hany Sobhi¹, Fred Nesbitt¹, Jamal Uddin^{1*}

¹Center for Nanotechnology, Department of Natural Sciences, Coppin State University, Baltimore, MD, USA

²Inorganic Synthesis Lab, Department of Natural Sciences, Coppin State University, Baltimore, MD, USA

Email: *juddin@coppin.edu, *tchavez-gil@coppin.edu

How to cite this paper: Ghann, W., Chavez-Gil, T., Goede, C.I., Kang, H., Khan, S., Sobhi, H., Nesbitt, F. and Uddin, J. (2017) Photophysical, Electrochemical and Photovoltaic Properties of Porphyrin-Based Dye Sensitized Solar Cell. *Advances in Materials Physics and Chemistry*, 7, 148-172. <https://doi.org/10.4236/ampc.2017.75013>

Received: March 23, 2017

Accepted: May 14, 2017

Published: May 17, 2017

Copyright © 2017 by authors and Scientific Research Publishing Inc.

This work is licensed under the Creative Commons Attribution International License (CC BY 4.0).

<http://creativecommons.org/licenses/by/4.0/>



Open Access

Abstract

Porphyrins occur in a number of important biomolecules and are also synthetically made for use as probe component of chemical and biological sensors. The performance of dye sensitized solar cells with two different porphyrin dyes was investigated in this work. The two porphyrin complexes comprised of a metal-free 5, 10, 15, 20-meso-tetrakis-(9H-2-fluorene-yl) porphyrin (H₂TFP) and its Zinc complex (ZnTFP). UV-Vis, Fluorescence, and Fourier transformed infrared measurements of the two dyes were carried out to evaluate their absorption, emission and binding characteristics. Both dyes absorbed light in the UV-visible region all the way to the near-infrared. The surface morphology and elemental analysis of the porphyrin dye sensitized photoanodes were determined using Field Emission Scanning Electron Microscopy Imaging and Transmission Electron Microscopy Imaging. Cyclic voltammetry studies, current-voltage characteristics and the electrochemical impedance spectroscopic studies were also carried out. Solar-to-electric energy efficiency of H₂TFP dye sensitized solar cell was higher (0.11%) than that of the zinc complex (0.08%). Thus the metal free porphyrin generated more power than the zinc complex under similar conditions. The impedance measurement also displayed less overall resistance for the free porphyrin (50 Ω) compared with the zinc complex (130 Ω). The LUMO levels of H₂TFP and ZnTFP sensitizers were -0.87 eV and -0.77 eV respectively. Both of these LUMO values are higher than the lower bound level of the conduction band of TiO₂ (-4.0 eV), ensuring the efficient injection of an electron from the excited porphyrin dye to the conduction band of the titanium dioxide.

Keywords

Porphyrin Dyes, UV-VIS, Fluorescence, Lifetime Decay, IR, FESEM, TEM, I-V, Cyclic Voltammetry, Impedance and DFT Calculation

1. Introduction

Dye sensitized solar cells (DSSCs) use dyes to absorb energy from the sunlight to produce excited electrons for the generation of electricity [1] [2] [3] [4] [5]. They are inexpensive, easy to produce and environmentally friendly. DSSCs are composed of a working electrode, usually a dye sensitized nanocrystalline TiO₂ on a conductive glass slide, a counter electrode, typically made of carbon or platinum on a conductive glass slide, and an electrolyte-a redox couple placed between the two electrodes for the regeneration of charge. Upon absorption of incident light, dye molecules are excited and subsequently relax by the injection electron into the conduction band of the TiO₂ semiconductor. Both natural pigments [6]-[12] and synthetic dyes [13] [14] [15] [16] have been used as photosensitizers for DSSCs. Here, two different porphyrins dyes have been used as photosensitizers for DSSC. Porphyrins are heterocyclic macrocycle organic compounds that usually bind with metals such as Magnesium and Ruthenium to form complexes. An example of naturally occurring porphyrins is the pigment, heme, found in red blood cells. It is also the basic structure of chlorophyll, the green pigment found in green plants. The large conjugation system of porphyrins allows for intense absorption in the visible region of the electromagnetic spectrum which makes them great candidates for use as photosensitizers in the construction of dye sensitized solar cell. Indeed, a number of studies on DSSCs with different types of porphyrins as photosensitizers have been reported [17]-[26].

In this work, a free base 5, 10, 15, 20-meso-tetrakis-(9H-2-fluorene-yl) porphyrin (H₂TFP) and its Zinc complex (Zn-TFP) have been synthesized and characterized to study the photo-physical and current-voltage properties of the DSSC.

2. Experimental Section

2.1. Materials and Methods

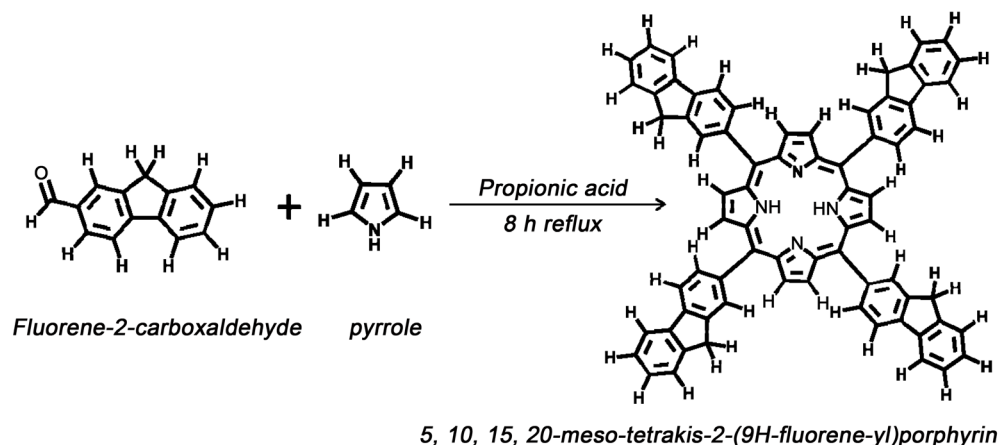
Reagents were purchased commercially and used as received, except for pyrrole and DMF that were redistilled by literature procedures [27]. All synthesis and air-sensitive characterization processes were carried out under a vacuum line and standard Schlenk techniques. Solvents for synthesis and spectroscopic characterization (ACS Grade) including dichloromethane (DCM), chloroform, hexanes, alcohols, and tetrahydrofuran were either purchased from Sigma-Aldrich, St. Louis, MO, or Across Organics, NJ, USA. Doubly purified deionized water from an 18 M Millipore system was used for aqueous solutions. N, N'-dimethylformamide (DMF) was distilled over calcium hydride under N₂ flow. Zn(OAc)₂·2H₂O was synthesized with high purity and checked through NMR spectrometry and melting point techniques. Column chromatography was carried out using silica gel 60, 230 - 400 mesh, from EMD Chemicals. The proton NMR spectrum was collected on a Bruker Avance III 400 MHz NMR spectrometer; FT-IR spectra were collected as KBr disk on a Nicolet iS50 FT-IR spectrometer; Electrochemistry determinations were collected in DMF solutions on a Princeton Applied Research VersaSTAT-3 potentiostat using a three electrode

cell unit. Steady-state absorbance spectra were measured on a Perkin Elmer Lambda 850 UV–visible (UV–vis) spectrophotometer and spectra were collected in DCM or chloroform solution. Elemental analyses were obtained from Galbraith laboratories Inc (Knoxville, TN). Titanium dioxide powder (Degussa P25) was purchased from the institute of chemical education. Fluorine tin oxide (FTO) conducting glass slides were purchased from Harford glass company, Hartford City, Indiana.

Steady-state fluorescence spectra were recorded on the fluorescence Nanolog Spectrofluorometer System from Horiba Scientific (FL3-22 iHR, Nanolog). The morphology of each film was analyzed using field emission scanning electron microscopy (FESEM; JSM-7100FA JEOL USA, Inc.). Transmission Electron Microscopy (TEM) images were acquired on JEM-1400 Plus (JEOL USA, Peabody, Massachusetts). The images were viewed using Digital Micrograph software from Gatan (Gatan, Inc, Pleasanton, CA). HOMO and LUMO calculations were carried out using Spartan'14 software from Wave function, Inc. Irvine, CA, and USA. TiO₂ paste was printed on FTO glass using WS-650 Series Spin Processor from Laurell Technologies Corporation.

2.2. Synthesis of 5, 10, 15, 20-Meso-Tetrakis-(9H-2-Fluorene-yl) Porphyrin

The synthesis of 5, 10, 15, 20-meso-tetrakis-(9H-2-fluorene-yl) porphyrin, denoted as H₂TFP, was carried out by the synthetic route shown in **Scheme 1**. In a 400 mL three-neck round-bottom flask equipped with a magnetic stirring bar and surmounted by a reflux condenser, freshly distilled pyrrole (1.45 g, 21.6 mmol), was added to a solution of fluorene-2-carboxaldehyde (4.2 g, 21.6 mmol), and propionic acid (180 mL) previously degassed through N₂. After reagents were mixed, the system was immersed in an oil bath and temperature was raised to 130°C. The reaction mixture was refluxed for 6 h to complete the reaction. The reaction progress was monitored by taking aliquots of the solution and recording its UV-vis spectra. After a constant pattern was observed for the Soret (=424 nm) and Q bands, the reaction was stopped, allowed to reach room

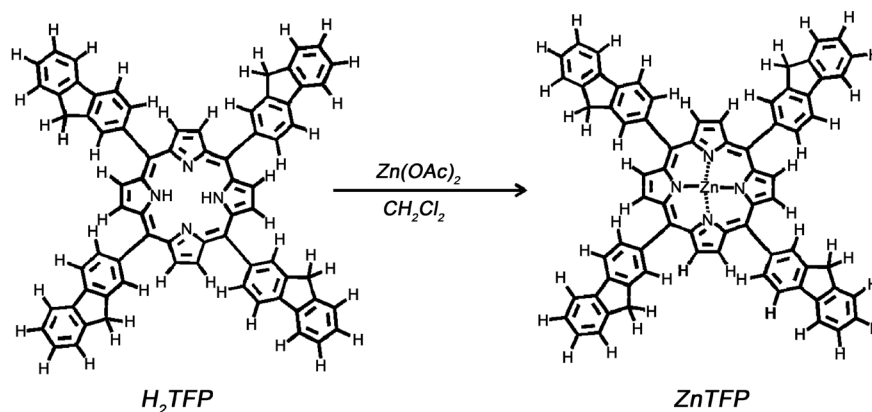


Scheme 1. Synthesis of H₂TFP freebase.

temperature and crunched ice added to precipitate a deep green-violet solid. The cold solution was filtered and the residue washed several times with methanol until no more colored solution was observed in the filtrate. The resulting tarry residue was triturated with toluene (50 ml) and allowed to stand in the refrigerator overnight. A fine purple powder was precipitated, filtered and washed thoroughly with cold toluene. The dried powder was dissolved in dichloromethane (100 ml), treated with trifluoroacetic acid (0.15 ml), and allowed to stir at room temperature for 4 h. The reaction mixture was refluxed for an additional 2.5 h and allowed to cool down to room temperature after which, a saturated solution of sodium carbonate, NaHCO_3 (100 mL) was added and the mixture was washed with water (2×100 mL) to attain an organic face after separation. Methanol (100 mL) was added over the organic layer to precipitate the free base H_2TFP that was collected by filtration, washed several times with cold methanol and dried in desiccator under CaCl_2 . The solid was dissolved in a little amount of dichloromethane (~ 7 mL) followed by purification on an alumina column. Eluting with pure dichloromethane then ensued affording a pure compound that was also characterized by UV-Vis giving a sharp Soret band at 424 nm. The solvent was evaporated on rotavapor system and the solid was re-dissolved once more in dichloromethane and filtered over cotton to remove any impurities. The filtrate was recovered in a vial and kept in a dark place at room temperature for several days under gentle evaporation, yielding a deep green-foiled material. Yield, 1.06 g (25.2%). Anal. Calcd for $\text{C}_{72}\text{H}_{46}\text{N}_4 \cdot \text{CH}_2\text{Cl}_2$, **H_2TFP** (MW = 967.22 g/mol): C, 83.32; H, 4.60; N, 5.32. Found: C, 83.31; H, 4.30; N, 5.61. **Figure 1** shows the NMR spectrum of H_2TFP . **$^1\text{H-NMR}$** (400 MHz, δ ppm (CDCl_3): 8.94 (s, 8H, $\text{CH}_{\beta\text{-pyrrolic}}$), 8.42 (s, 4H, $\text{H}_{\text{fluorenyl}}$, H_1), 8.28 (d, 4H, $J_{\text{HH}} = 0.1$ Hz, $\text{H}_{\text{fluorenyl}}$, H_4), 8.17 (d, 4H, $J_{\text{HH}} = 0.02$ Hz, $\text{H}_{\text{fluorenyl}}$, H_3), 8.07 (d, 4H, $J_{\text{HH}} = 0.02$ Hz, $\text{H}_{\text{fluorenyl}}$, H_5), 7.72 (d, 4H, $J_{\text{HH}} = 0.2$ Hz, $\text{H}_{\text{fluorenyl}}$, H_8), 7.55 (t, 4H, $\text{H}_{\text{fluorenyl}}$, H_6), 7.46 (t, 4H, $\text{H}_{\text{fluorenyl}}$, H_7), 7.24 (strong 1H, CDCl_3), 5.43 (s, 2H, dichloromethane-trace), 4.22 (s, 8H, $4\text{CH}_{2\text{-fluorenyl}}$), and -1.36 (s 2H, $\text{H}_{\alpha\text{-pyrrolic}}$, not shown). **FT-IR** (KBr disk, ν/cm^{-1}): 3438 m, 3044 m, 2894 w, 1706 s, 1553 m, 1456 m, 1401 w, 1298br, UV-vis (CH_2Cl_2) 413, 507, 536, 583, 637 nm. 1226 w, 1049 w, 1004 w, 972 w, 800 w, 765 m, 734 s, 422 w. **UV-vis** DCM(λ , nm), (ϵ , $10^5 \text{ M}^{-1} \text{ cm}^{-1}$): 424 (Soret), 518, 554, 591, 649 (Qs).

2.3. Complex Zn-5, 10, 15, 20-Meso-Tetrakis-(9H-2-Fluorene-yl)Porphyrinato(II)

Zn-5, 10, 15, 20-meso-tetrakis-(9H-2-fluorene-yl) porphyrinato (II), denoted as ZnTFP, was prepared according to the synthetic route shown in **Scheme 2**. In a 50 mL two-neck round-bottom flask, 50 mg (0.22 mmol) of $\text{Zn}(\text{Oac})_2 \cdot 2\text{H}_2\text{O}$ was dissolved in 25 mL dichloromethane previously degassed under anitrogen atmosphere for 10 minutes. To this solution, 21 mg (0.02 mmol) of 5, 10, 15, 20-meso-tetrakis-(9H-2-fluorene-yl) porphyrin was added and degassed with nitrogen for about 10 min. Under these conditions, the reaction flask was capped with rubber septum and kept stirring for 12 h protected from light. After that period the flask was connected to a reflux condenser surmounted by a CaCl_2 trap



Scheme 2. Synthesis of Zinc-porphyrin complex.

and refluxed for more two additional hours. The solvent was evaporated and the resulting solid dried overnight on desiccator and dissolved in dichloro-methane. This solution was washed with a concentrated sodium hydrogen carbonate (10% solution, 100 mL) and after separation the resulting organic phase was dried on sodium sulfate anhydrous for 4 h protected from light. The solvent was evaporated and the solid dissolved in a small amount of dichloromethane. Silica gel was used for flash filtration employing dichloromethane: methanol (9:1 v/v) as eluent solution. After solvent evaporation, the solid was treated with dichloro-methane (~10 mL), and filtered on cotton to remove any remaining impurities. The filtrate was recovered in a vial, placed inside of a flask capped with rubber septum under an atmosphere of methanol and left to stand for several days at room temperature protected from light. The obtained blue wish-violet solid was washed twice with cold methanol and dried in vacuum over fused CaCl_2 . The yield was 19.3 mg (88%). Anal. Calcd for $\text{C}_{72}\text{H}_{44}\text{N}_4\text{Zn}$ (1030.61g/mol): C, 83.90; H, 4.31; N, 5.44; Zn, 6.34; Found: C, 82.62; H, 6.18; N, 3.49; Zn, 2.57. The $^1\text{H-NMR}$ spectrum of this compound is displayed in **Figure 2**. $^1\text{H-NMR}$ (400 MHz, δ ppm (CDCl_3): 9.08 (s, 8H, $\text{CH}_{\beta\text{-pyrrolic}}$), 8.42 (s, 4H, $\text{H}_{\text{fluorenyl}}$, H_1), 8.28 (d, 4H, $J_{\text{HH}} = 0.1$ Hz, $\text{H}_{\text{fluorenyl}}$, H_4), 8.17 (d, 4H, $J_{\text{HH}} = 0.02$ Hz, $\text{H}_{\text{fluorenyl}}$, H_3), 8.07 (d, 4H, $J_{\text{HH}} = 0.02$ Hz, $\text{H}_{\text{fluorenyl}}$, H_5), 7.72 (d, 4H, $J_{\text{HH}} = 0.2$ Hz, $\text{H}_{\text{fluorenyl}}$, H_8), 7.55 (t, 4H, $\text{H}_{\text{fluorenyl}}$, H_6), 7.46 (t, 4H, $\text{H}_{\text{fluorenyl}}$, H_7), 5.43 (s, 8H, $\text{CH}_{\beta\text{-pyrrolic}}$), and 4.22 (s, 8H, $4\text{CH}_{2\text{-fluorenyl}}$). **FTIR** (cm^{-1} , KBr): 2920 s, 2850 sh, 1710 m, 1460 s, 1400 w, 1340 m, 1280 m, 1220 m, 1000 m, 802 w, 476 w, 422 w. **UV-vis** (nm, dichloromethane), 427 (Soret); 552, 592 (Qs); 267 $\pi\text{-}\pi^*$ fluorenyl moieties.

2.4. Fluorescence Lifetime Measurements

The dye samples were dissolved in 3 mL of ethanol for fluorescence lifetime solution. To prevent inner filter effect, absorption measurements were carried out to ensure that the absorbances of the dyes were less or equal to 0.15 absorbance unit. Fluorescence decay was measured using Horiba Deltaflex fluorescence lifetime system using the time-correlated single-photon counting (TCSPC) technique with the PPD-850 picosecond photon detection module. The excitation source was 340 nm light-emitting diodes (Delta LED).

2.5. Fabrication of Solar Cell

The photoanode was prepared by depositing a thin film of TiO₂ on the conductive side of fluorine doped tin oxide (FTO) glass using a spin coater and sintered at 380 °C for 2 hours [8] [9]. The TiO₂ covered FTO glass was then immersed in a freshly prepared 5 mM dye solution for a period of two hours. The counter electrode (cathode) was prepared by painting FTO glass with colloidal graphite. The dye-sensitized electrode and the carbon electrode were assembled to form a solar cell sandwiched with a redox (I⁻/I³⁻) electrolyte solution. The active area of the cell was 5 cm².

2.6. Photovoltaic Properties Measurement

The energy efficiencies of the fabricated DSSCs were measured using 150 W fully reflective solar simulator with a standard illumination with air-mass 1.5 global filter (AM 1.5 G) having an irradiance corresponding to 1 sun (100 mW/cm²) purchased from Sciencetech Inc., London, Ontario, Canada and Reference 600 Potentiostat/Galvanostat/ZRA from Gamry Instruments (734 Louis Drive, Warminster, PA 18974). The tested solar cells were masked to an area of 5 cm². Each cell performance value was taken as the average of three independent samples. The solar energy to electricity conversion efficiency (η) was calculated based on the equation:

$$\eta = FF \times I_{sc} \times V_{oc} \quad (1)$$

where, FF is the fill factor, I_{sc} is the short-circuit photocurrent density (mA cm⁻²), and V_{oc} is the open-circuit voltage (V) as listed in **Table 3**.

3. Results and Discussion

3.1. ¹H NMR Spectra

The proton NMR signals of free base H₂TFP is depicted in **Figure 1**. In its β and *meso* positions are found the exocyclic protons with respect to the macrocyclic and local pyrrole currents which experience the deshielding influence of the latter. The signals for these protons are observed at low field (δ from 7.46 to 8.42 ppm for the meso-fluorenylprotons and at δ from 8.5 to 8.9 ppm for the β -pyrrole protons). The protons of the N-H groups are exocyclic with respect to the local ring currents and endo-cyclic with respect to the macrocyclic current. Thus, the shielding effect of the latter prevails and the signals for the protons of the N-H groups are observed at very high field (from δ -1.4 to -4.4 ppm). [28] The proton NMR spectra of the metallic fluorenylporphyrins show clear differences relative to the free base fluorenylporphyrin. Upon complexation of the free base H₂TFP with zinc-acetate, the H _{β} protons of pyrrole ring (in H₂TFP at δ , 8.94 ppm) were shifted downfield (to δ 9.03 ppm). The inner imino hydrogens appear as a singlet at -2.60 ppm, relative to -2.75 ppm for H₂TFP [28]. Thus the chemical shifts of ¹H-NMR of free-base H₂TFP especially for N-H protons, clearly shows the effect of non-planarity on the spectra of zinc-fluorenylporphyrin. In the neutral free base H₂TFP, for example, the H _{α} and H _{β} signals appeared at δ

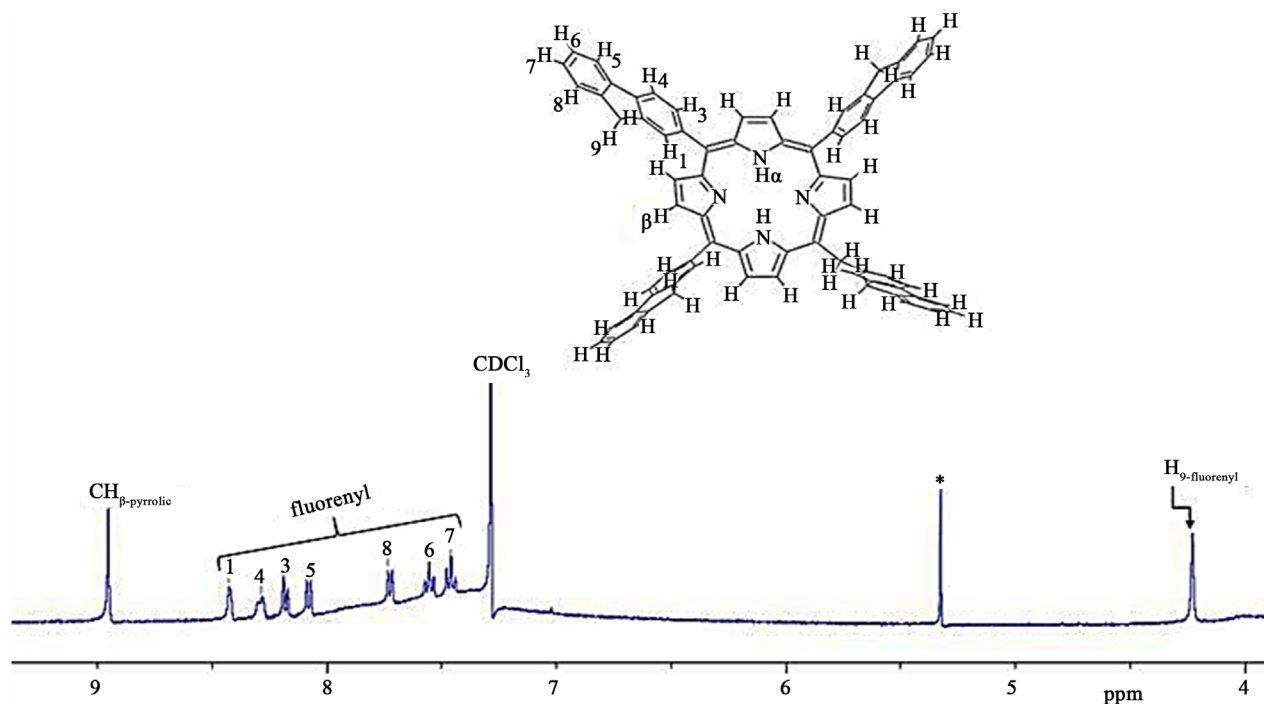


Figure 1. ^1H -NMR spectra of free base 5, 10, 15, 20-*meso*-tetrakis-(9*H*-2-fluorene-yl) porphyrin, (H_2TFP) with proton numbering for clarity, 1.0 mM chloroform- d . Starred peaks are solvent impurities.

–2.60 and 8.94 ppm, respectively, while in the zinc-porphyrin complex (**Figure 2**), which has a severely distorted geometry with the H_β signal substituted and the slighted low field shifted H_β protons that appears as a quasi-doublet at $\delta 9.08$ ppm. Those variations in the proton NMR spectra are ascribed to the energy cost on the non-planar distortion geometry depicted by the porphyrin structure during its complexes formation. The difference between these protons in regard to their intensity and signal splitting is related to the geometry instead of molecular symmetry [29] [30].

3.2. Electronic Absorption Spectra

The UV-visible absorption spectra in dichloromethane of the neutral free base (H_2TFP) and its Zinc complex (ZnTFP) were carried out at room temperature and have been reported previously [31]. The measurements of these compounds were performed at different concentrations due to the difference in their absorption intensities; a more concentrated solution was used to display the Q bands and a less concentrated for the Soret band absorption of free and metallic porphyrin. The UV-visible spectra of neutral free base H_2TFP exhibit an intense Soret band with a maximum absorption around 424 nm and four Q bands characteristic of a porphyrin free base which are located at 521, 556, and 598 and at 654 nm, respectively. In addition, there is a wide and strong absorption band around 267 nm, assigned to the π - π^* intramolecular transitions of fluorenyl dyes if compared with the weak absorption in the UV range which is clearly apparent but absent for Tetra-Phenyl-Porphyrin (TPP) [31]. The absorption at 424 nm

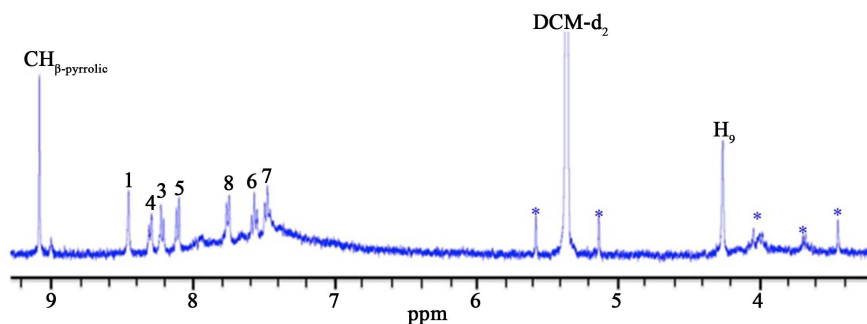


Figure 2. $^1\text{H-NMR}$ spectra of zinc-fluorenylporphyrin complex 1.5×10^{-5} M–dichloromethane- d_2 at 298 K. Starred peaks are solvent impurities.

corresponding to the B(0, 0) band (Soret band, $\epsilon = 2.3 \times 10^5 \text{ M}^{-1} \text{ cm}^{-1}$) is slightly red shifted compared to 417 nm for TPP. This tendency in red shifting is also observed for the four Q bands. The metallic porphyrin complexes in the other hand, exhibit characteristic changes on the electronic spectra compared to H_2TFP .

Thus, the absorption spectra of Zn(II) porphyrin complex display a single Soret band which is a combination of the Q_x and Q_y electronic transitions due to the D_4h symmetry of metallic porphyrins, instead of the D_2h low symmetry characteristic of free base porphyrins, with two discernible sub-bands ($\text{Q}_{(1,0)}$ and $\text{Q}_{(0,0)}$) [32] [33]. Thus, the zinc-porphyrin exhibit an intense and red shifted band at 426 nm (Soret), $\epsilon = 3.8 \times 10^5 \text{ M}^{-1} \text{ cm}^{-1}$, together with two Q-bands in the visible range, one of moderated intensity located at 554 nm ($\text{Q}_{1,0}$) attributed to a vibration component which is responsible in the withdrawn of intensity of the Soret band, however its molar absorptivity is almost constant in metallo-porphyrins. A second Q-band is observed at 595 nm ($\text{Q}_{0,0}$) which intensity in free-base porphyrins is defined for the difference between the transitions of two orbitals (a_{1u} and a_{2u} orbitals) that lead to E_u state, but if they are degenerated as occur in metallic-porphyrins this band practically does not exist [34] (Figure 3). An additional broad band is observed in the UV range which corresponds to $\pi\text{-}\pi^*$ absorption of the fluorenyl dyes. This absorption at 310 nm has different intensity than for the zinc complex as well for the free base H_2TFP as consequence of the difference in electron's donor/withdraw exerted for the fluorenyl groups on the porphyrin chromophore geometrical conformation (distorted, freebase; butterfly zinc complex). Also, a slightly red shift on the UV band from 268 nm to 271 nm shows a deeply change in the metallic porphyrin derivative due to the remarkable geometry changes on the 5, 10, 15, 20-mesofluorenyl positions on the porphyrin ring.

3.3. Steady State Fluorescence Studies

Fluorescence spectra of H_2TFP and ZnTFP deployed in the fabrication of the DSSC were measured to investigate their emission characteristics. The spectra measured in dichloromethane by scanning from 500 to 800 nm with fixed excitation at 420 nm are displayed in Figure 4. Each of the dyes displayed different fluorescence behavior according with its chemical composition. Thus, the

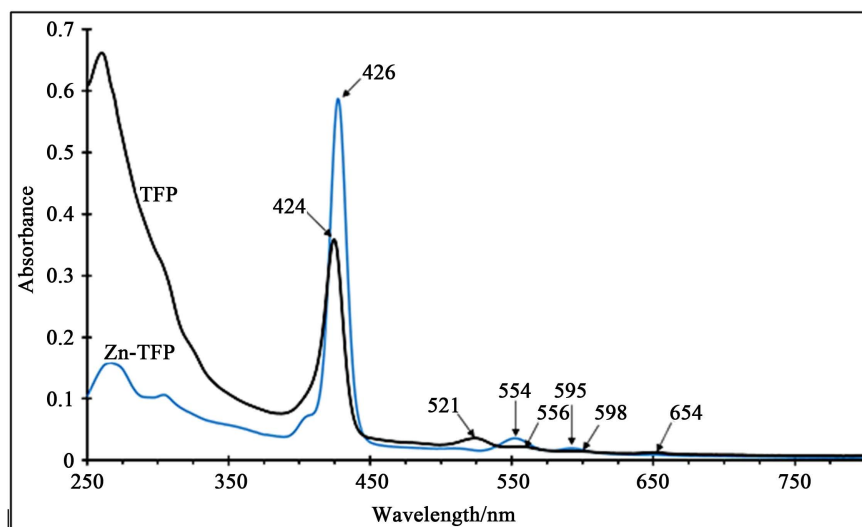


Figure 3. UV-VIS spectra of free base 5, 10, 15, 20-*meso*-tetrakis-(9*H*-2-fluorene-yl) porphyrin, **1** (H_2 TFP), and Zn-5, 10, 15, 20-*meso*-tetrakis-(9*H*-2-fluorene-yl) porphyrinato (II) in dichloromethane.

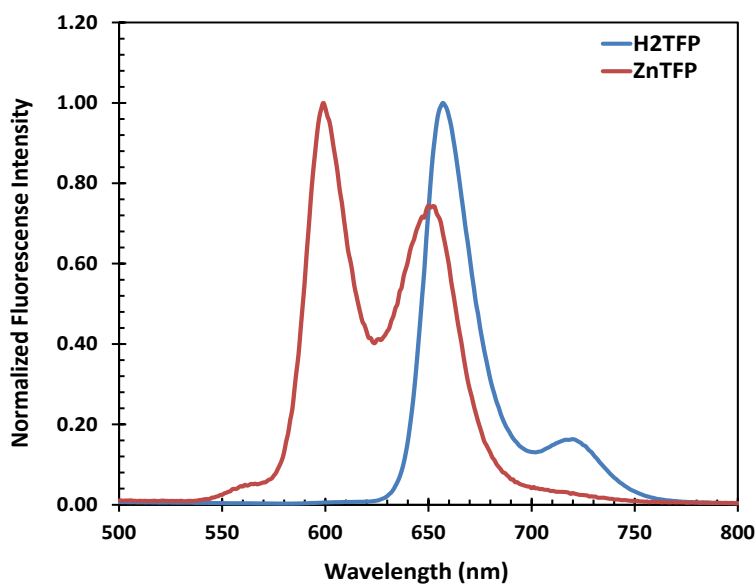


Figure 4. Fluorescence spectra of free base 5, 10, 15, 20-*meso*-tetrakis-(9*H*-2-fluorene-yl) porphyrin, **1** (H_2 TFP), and Zn-5, 10, 15, 20-*meso*-tetrakis-(9*H*-2-fluorene-yl) porphyrinato (II) in dichloromethane.

emission pattern of the free porphyrin resembles its UV-Vis absorption spectrum but the emission observed with the Zn complex shows to be very different. H_2 TFP for example, displayed a red shift while ZnTFP exhibited a broadened fluorescence spectrum. The two emission peaks for the H_2 TFP occurred at 658 nm and 720 nm, whereas the fluorescence bands for ZnTFP occurred at 599 nm and 650 nm, respectively. It could also be observed from the absorption spectra that the fluorescence peaks are the result of the metallic substitution that occurred on the first Q-bands of the porphyrin and these transitions are not dependent on the Soret band.

3.4. Fluorescence Lifetime Measurement

As part of the photophysical studies on the porphyrin dyes, the fluorescence lifetime measurement were carried out to determine the length of time the porphyrin molecules stay in the excited state before decay. **Figure 5** and **Table 1** show the fluorescence lifetime of the free-base (H_2TFP) and the Zinc complex ($ZnTFP$). The fluorescence decay profiles were analyzed by two-exponential fit giving two components with lifetimes of 38.91 ps and 1.38 ns for the free porphyrin and 58.11 ps and 5.27 ns for the zinc complex. The two lifetime is an indication of presence of two different species that decay at different rates. In dye sensitized solar cells the electrons from the excited state are injected into the conduction band of titanium dioxide on which they dye is anchored. The injection process is also in competition with the normal relaxation pathways of the fluorophore in the excited state. Thus, understanding the decay process may help predict the fate of the electron in the excited state. Most organic molecules including porphyrin have short fluorescence lifetime which could easily be quenched by the iodide/triiodide redox couple. Therefore dye molecules with short lifetime are more likely to have a short lifetime in the presence of the electrolyte.

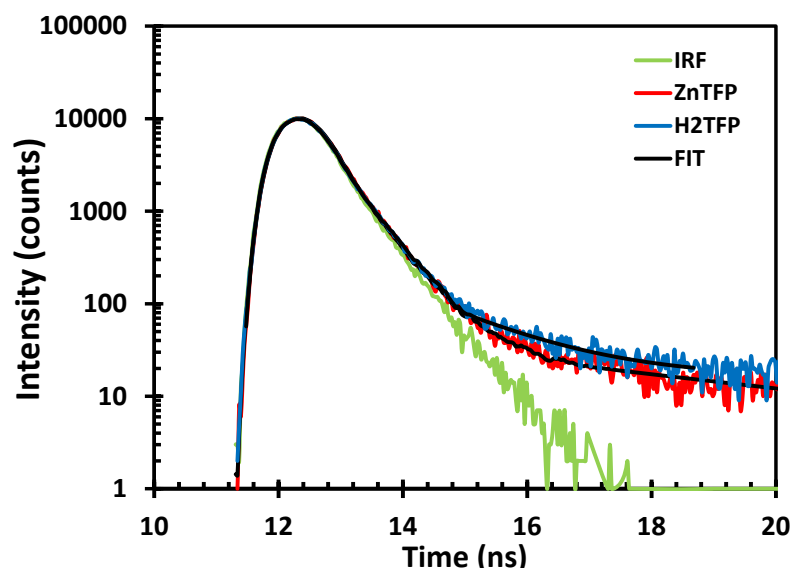


Figure 5. Fluorescence lifetime measurement of free base 5, 10, 15, 20-*meso-tetrakis*-(9*H*-2-*fluorene-yl*) porphyrin, 1 (H_2TFP), and Zn-5, 10, 15, 20-*meso-tetrakis*-(9*H*-2-*fluorene-yl*) porphyrinato (II) in dichloromethane.

Table 1. Fluorescence lifetime measurement of cyanine dyes free base 5, 10, 15, 20-*meso-tetrakis*-(9*H*-2-*fluorene-yl*) porphyrin, 1 (H_2TFP), and Zn-5, 10, 15, 20-*meso-tetrakis*-(9*H*-2-*fluorene-yl*) porphyrinato (II) in dichloromethane.

Sample Name	Lifetime (ps)		
	τ_1 (ps)	τ_2 (ns)	χ^2
H_2TFP	38.91	1.38	1.10
ZnTFP	58.11	5.27	1.09

3.5. FT-IR Spectroscopy

The FT-IR of the H_2TFP and $ZnTFP$ are displayed in **Figure 6**. In the free base, H_2TFP , the moderate IR bands at 3433 and 1540 cm^{-1} are attributed to the NH stretching vibrations, but they were absent in the spectra of the complexes, because the hydrogen atom in the N–H bond were replaced by a transition metal ion. [35] The skeletal vibrations of the free porphyrin ring appear at 1553 and 1288 cm^{-1} , respectively. A band of moderate intensity at 1450 cm^{-1} corresponds to (C–C) stretching of the fluorenyl dyes, and other two weak bands at 3030 and 2890 cm^{-1} are ascribed to the stretching of (9H) fluorenyl and (H_β) pyrrolic hydrogen, respectively. The vibrations implicated below $\sim 1000\text{ cm}^{-1}$ generally entail out-of-plane stretching for C–C and C–H groups in the fluorenyl chromophore. Additionally, combination bands in the $1500 - 500\text{ cm}^{-1}$ region involving non-planar C–H vibrations have been reported previously for the fluorene dye [36] [37] [38] [39]. The IR results with Zn(II) metalloporphyrins, implies deep changes on the strong stretching composed by the two bands at 733 and 744 cm^{-1} observed for the H_2TFP free base. On the Zn(II) metalloporphyrins ($ZnTFP$), these stretchings were splitted into two weak bands shifted to 760 and 690 cm^{-1} . Thus, the difference of energy between the splitted signals for $ZnTFP$ are minimal. These results are still directly related with the cost of stabilization energy encountered in the formation of metallic heterocyclic complexes.

3.6. Field Emission Electron Microscopy (FESEM) Studies

Studies on the morphology of the TiO_2 electrode were further investigated using Field-Emission Scanning Microscopy Imaging (FESEM). **Figure 7** shows the FESEM microscopic morphology of the porphyrin dye adsorbed nanocrystalline

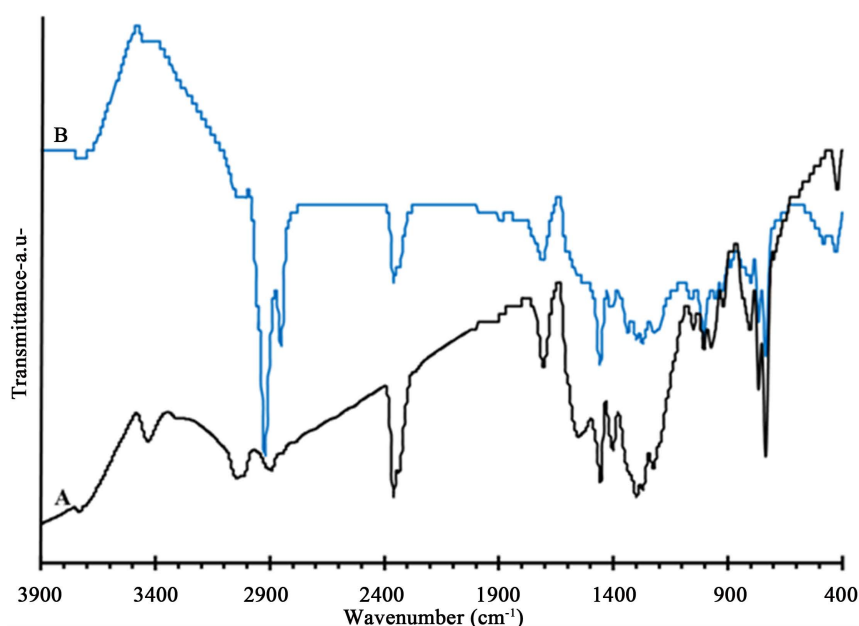


Figure 6. FT-IR spectra of (a) 5, 10, 15, 20-meso-tetrakis-(9H-2-fluorene-yl)porphyrin, H_2TFP (a), and (b) zinc-5, 10, 15, 20-meso-tetrakis-2-(9H-fluorenyl)porphyrinato (II), $Zn-TFP$ (b), (KBr disk).

TiO₂ film. Only minor changes are observed in the surface morphology of the samples before and after dye application. The dye adsorbed TiO₂ was finer than the bare TiO₂ nanocrystalline film. Energy dispersive X-ray spectroscopic (EDS) mapping analysis of a nanocrystalline TiO₂ partially sensitized with porphyrin dye is displayed in **Figure 7(a)**. The part of the film containing the dye shows prominent peak for carbon, the predominant element in porphyrin. The peak for carbon is negligible in the part of the film without the porphyrin, instead the prominent titanium peaks are observed. EDS was also used for the chemical characterization of the porphyrin sensitized TiO₂ in comparison with the bare TiO₂ film. An intense carbon peak was observed in the spectrum of porphyrin dye-sensitized TiO₂ film (**Figure 7(b)**) compared to the barely visible carbon peak in the spectrum of the bare TiO₂ (**Figure 7(c)**). Thus the results are consistent with the elemental composition of free porphyrin which is mainly

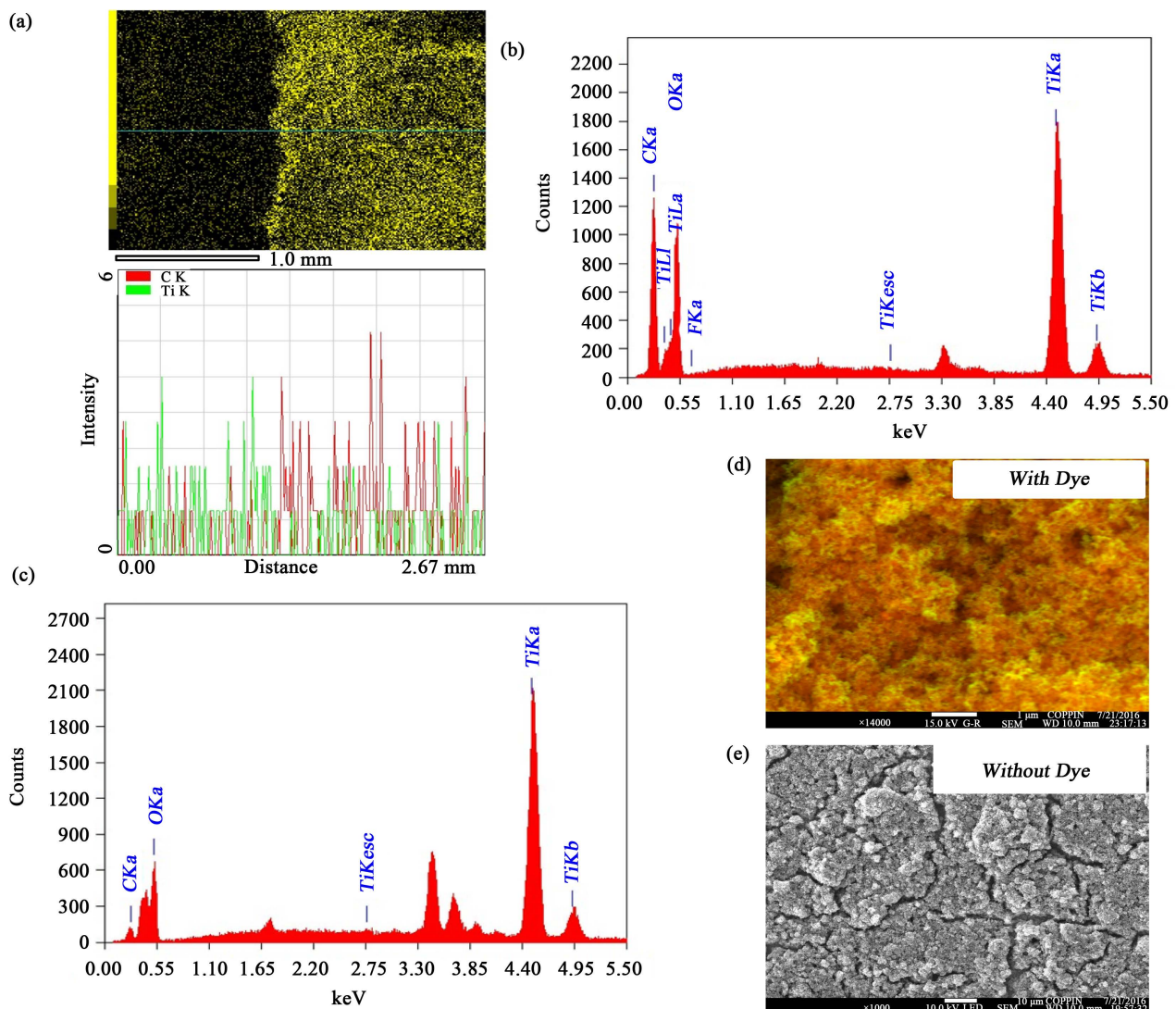


Figure 7. Field emission scanning electron microscopy and energy dispersive x-ray studies: (a) line profile analysis of a partially dyed TiO₂ film on FTO glass (b) EDS spectrum of porphyrin dye sensitized TiO₂ on FTO glass (c) EDS spectrum of bare TiO₂ coated FTO glass (d) FESEM image of porphyrin dye sensitized TiO₂ film (e) FESEM image of bare TiO₂ coated FTO glass.

made up of carbon. The nanocrystalline nature of the TiO_2 which increases the surface area of the titanium dioxide is clearly observed in **Figure 7(d)** and **Figure 7(e)**. The increased surface area allows more dye molecules to be anchored on it which ultimately increase the efficiency of the solar cell.

3.7. Transmission Electron Microscopy Imaging Studies

To confirm the adsorption of the porphyrin dyes on the TiO_2 nanoparticles, the high-resolution images were taken by transmission electron microscopy as shown in **Figure 8**. To get the TEM images, the porphyrin dye powder was dissolved in acetone and the resulting solution filtered with a filter paper (VWR.com, grade 410) to remove residues. After that, TiO_2 powder was added to form a mixture with the filtered dye solution. The mixture was then suspended for 20 min to ensure the adsorption of the dye into the TiO_2 . A drop of the dye mixture was subsequently deposited on a TEM grid and allowed to dry inside a hood overnight. A mixture of TiO_2 and acetone was dried on another TEM grid and used as an external control. Anatase TiO_2 nanoparticles were observed with a particle size range of 20 - 25 nm as shown in **Figure 8**. In **Figure 8(a)** and **Figure 8(b)**, the small spherical dyes of 1 - 3 nm were observed on the anatase TiO_2 particles (the arrows in the images are guide to the dyes). Conversely, dye particles were not observed in the control as shown in **Figure 8(c)**. **Figure 8(d)** and **Figure 8(e)** are a zoom-in images of one of the TiO_2 crystals and its FFT pattern, respectively. The interplanar distance in the TiO_2 crystal obtained by Fourier transform was 0.34 nm corresponding to the (101) plane of

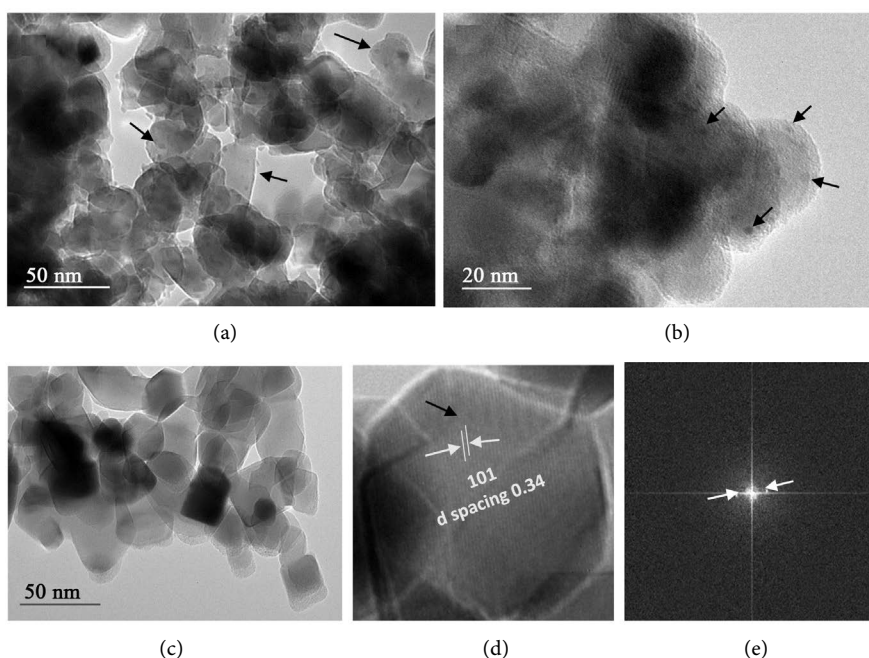


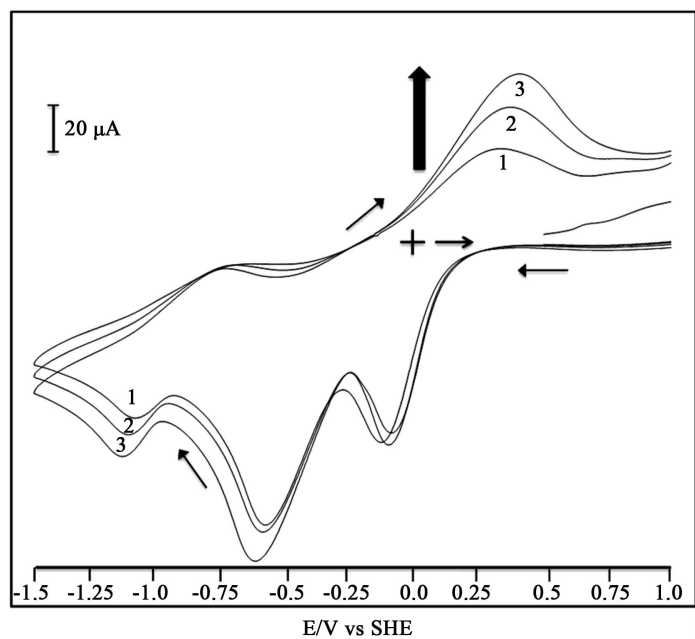
Figure 8. High-resolution TEM images of the porphyrin dye/ TiO_2 samples and the TiO_2 nanoparticles. (a) and (b) high resolution TEM images of porphyrin dye/ TiO_2 ; and (c) of TiO_2 nanoparticles without dye (d) zoom-in image of one of the TiO_2 crystals (c), and (e) the FFT pattern of the zoom-in image.

the anatase TiO₂ powder. It is speculated that the adsorption between the TiO₂ nanoparticles and the dyes results from the electrostatic binding, since the dyes do not have any functional groups which are able to induce any binding between them.

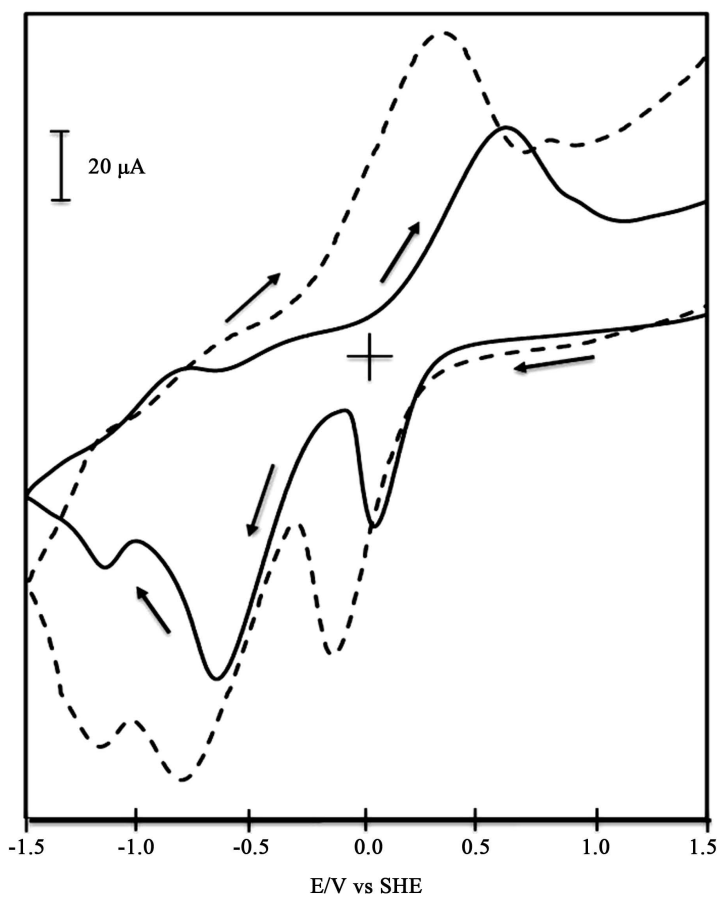
3.8. Cyclic Voltammetry

The standard redox process of a free base porphyrin is characterized for the two-electron transfer reaction with two reversible waves named E¹Ox and E²Ox, which are determinate by cyclic voltammetry. [40] The voltammogram of meso-tetrakis-phenyl porphyrin (TPP) had been used as a standard to interpret the electron transfer process that occurs on a large number of freebase and metallic porphyrins [41]. It is worth to mention that wave potentials on the *meso* positions are deeply affected by substituents around the porphyrin heterocyclic ring. In addition, the type of metal (hard or soft) and the degree of its oxidation state are directly related with the electron transfer changes on metallic porphyrins [42]. Felton *et al.* demonstrated that most of metallic porphyrins exhibit a constant potential difference between the first and the second macrocycle centered oxidation, or on the first and second macrocycle centered reductions. [43] Cyclic voltammetry, CV, for free base H₂TFP and its metallic derivatives were recorded using a one-compartment three-electrode cell, equipped with a platinum, Pt, disk working electrode from Basi-Analytical Instruments (1.6 mm diameter), a platinum wire as auxiliary electrode, and all potentials were referenced to Ag/AgNO₃ (0.10 M, in acetonitrile) electrode. The working electrode was polished first using 0.30 μm followed by 0.05 μm alumina polish (BASi). The supporting electrolyte was 0.1 M tetrabutylammonium perchlorate (NBu₄ClO₄) and the measurements were made in N, N'-dimethylformamide, DMF. All potentials were converted to the SHE scale by adding 0.50 V to the experimental data [44].

The cyclic voltammetry were carried out on a Princeton Applied Research Versa STAT-3 potentiostat with samples degassed under a nitrogen flow before each scan. The synthesis and characterization of meso-tetrakis-fluorenylporphyrin, H₂TFP, in **Scheme 1**, has been previously reported [45] and for comparative purposes, the electrochemical and spectroscopic results of this chromophore and its metallic complexes are included in this study [46] [47]. The cyclic voltammogram of free base H₂TFP in a 0.1 M Bu₄NClO₄/DMF solution is illustrated in **Figure 9(a)** and summarized in **Table 2**. The CV of free base was recorded by applying three cycles, which shows two reversible redox couples with a peak potential, $E_{1/2}^o = +0.31$ V and at $E_{1/2}^o = -0.79$ V versus SHE. These two reversible reactions that occur at slightly different regions, correspond to the successive one electron redox reaction on the porphyrinic ring. The voltammogram shows another irreversible, strong, and broad wave at $E_{1/2}^o = -0.56$ V that correspond at two electron transference reaction, attributed to the meso-fluorenylmoieties. This attribution is in agreement with similar meso-tetrakis aromatic-porphyrins that shows identical electrochemical pattern according with Spiro *et al.* [48]. In addition, the successive redox cycles applied on the same sample and at different scan rates do not shows great changes on the electrochemistry



(a)



(b)

Figure 9. Cyclic voltammograms of (a) H_2TFP and (b) ZnTFP ; $1.0 \times 10^{-6} \text{ mol dm}^{-3}$, $\text{N, N}'$ -dimethylformamide, 0.1 mol dm^{-3} tetrabutylammonium perchlorate. Scan rate $50 \text{ mV} \cdot \text{s}^{-1}$ (a) three cycles, and (b) $\text{Zn-TFP} + 0.1 \mu\text{M}$ of pyridine, (dashed line). Potentials recorded vs. Ag/AgNO_3 (0.1 M) reference electrode and converted to SHE by addition of 0.5 V .

Table 2. Redox potentials for free base H₂TfP, and metallic [ZnTfP]²⁺ complex.

Compound	E _{1/2} (V) ^a	Assignment
H ₂ TfP	-0.07	Por 0/+
	0.31	Por +/-
	-0.56	Fluorenyl 0/+
	-1.07	Por +/2+
	-0.79	Por 2+/+
Zn-TfP	0.57	Zn II/III
	0.03	Zn III/II
	-0.63	Fluorenyl 0/+
	-0.86	Por 0/+
	-1.12	Por +/0
Zn-TfP + pyridine	0.36	Zn II/III
	-0.13	Zn III/II
	-0.77	Fluorenyl 0/+
	-1.19	Por 0/+
	-1.13	Por +/0

^aPotentials reported versus the SHE reference electrode in acetonitrile (0.1 M) with samples dissolved in DMF. Scans recorded at 100 mV·s⁻¹ and 25°C.

behavior, that could be related with the high stability showed by this porphyrin when exposed to air for long times but light protected. The peak potential separations E_p between the anodic and cathodic peaks than for H₂TfP and its complexes ranged from 53 mV to 67 mV with an average of 61 ± 0.002 mV. These values are close to the theoretical value of 59 mV for a one-electron transfer reaction, that for a reversible process the peak width is given by the following relationship:

$$E_{p/2} - E_p = 2.2 \left[\frac{RT}{nF} \right] \quad (2)$$

where $E_{p/2}$ is the half-peak potential at the half value of the peak current, E_p is the peak potential, F is the Faraday constant and n is the number of electrons in the reaction. The presence of metallic ions in the fluorenylporphyrin core makes the oxidation reaction of these complexes easier with the redox potentials shifted towards lower values.

The results of our experiments shows that zinc-fluorenyl porphyrin complex (ZnTfP) undergoes a one electron transfer process with a half wave potential, $E_{p/2}^o = 0.57$ V vs SHE in DMF (**Figure 9(a)**) for oxidation; while the reduction reaction shows to occur at $E_{p/2}^o = 0.03$ V vs SHE in a reversible one electron transfer as indicated by the peak current ratio, i_a/i_c which is close to unity (herein, 1.0) at the scan rates investigated (50 - 100 mV/s). The peak separation between the anodic and cathodic peak potentials, $E_{pa} - E_{pc}$, shows to be close to

0.53 V (one electron transfer), which is attributed to a reversible electrochemistry process [49]. Thus, the one electron donating/withdrawing in a symmetrical process (among its reversible characteristic), means that this material is very stable. Some broadening occurred, however, due to uncompensated resistance. Similar as observed on other free base porphyrins, the fluorenyl group on the pyrrolic ring makes ZnTFP easier to reduce [50]. Therefore, the presence of aromatic groups in the meso positions weakens the interaction between the metal and porphyrin by turning easier the electron transfer reactions. In addition, cyclic voltammograms were recorded after the addition of a diluted pyridine solution (1.25 μM , see Figure 9(b)-dotted curve), in that a symmetrical shift to low potentials with $\Delta E_{1/2}^p = 0.21$ V and $\Delta E_{1/2}^c = 0.27$ V ascribed to the oxidation of the Zn^{III} ion. This process occur in parallel to the raise of well defined peak current ratio, i_a/i_c ($\Delta i = 12$ μA) attributed to an enhancement in the zinc-complex geometry (O_h), instead of the butterfly associated with the square planar coordination.

3.9. I-V Performance

Figure 10 and Table 3 show the current-voltage characteristics the free base, H_2TFP , and metallic meso-tetrakis-2-(H9-fluorenyl) porphyrin. The current-voltage curves reveal a significant difference in the photovoltaic performance of the free base porphyrin (H_2TFP) and ZnTFP sensitized solar cell. A higher efficiency was obtained from devices fabricated with the free porphyrin

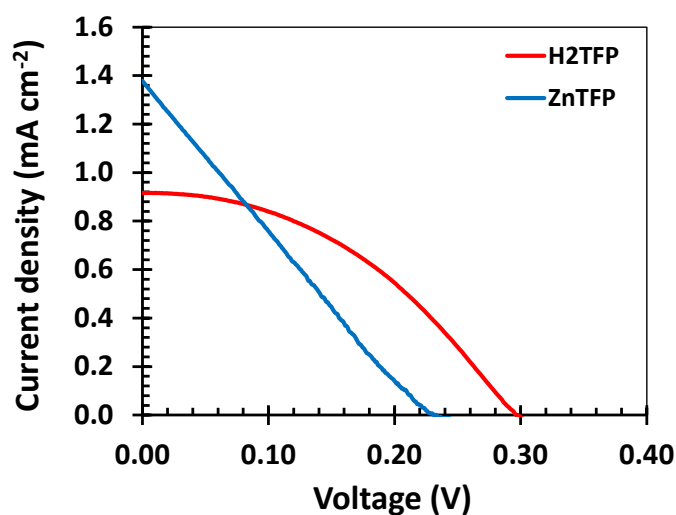


Figure 10. Current and Voltage Characteristics of dye sensitized solar cells fabricated with free base H_2TFP and metallic meso-tetrakis-2-(H9-fluorenyl) porphyrin coordinated to $\text{Zn}(\text{II})$.

Table 3. Current and voltage characteristics for the porphyrin dye sensitized solar cells.

DYE	Isc (mA/cm ²)	Voc (V)	Imp (mA/cm ²)	Vmp (V)	Fill Factor	Efficiency (%)
H_2TFP	0.92	0.31	0.64	0.18	0.40	0.11
ZnTFP	1.38	0.25	0.72	0.11	0.23	0.08

(0.11%) compared with that fabricated with Zn complex (0.08%). The higher efficiency of the free porphyrin compared to the Zn complex could be due to an efficient interaction between the TiO₂ surface and the free porphyrin. Such interaction favors the injection of electron from the dye into the conduction band of the titanium dioxide. Specifically,, the geometry orientation and flexibility changes when the metal is inserted into the porphyrin ring. Thus, the rigidity of the resulting coordinated porphyrin reduces the interaction of the dye with the TiO₂ surface leading to a decrease in the electron transfer efficiency of the cell. Therefore, the efficiency values on these dyes could be improved when anchoring groups that facilitate charge transfers attached to these porphyrin molecules.

3.10. Electrochemical Impedance Spectroscopy

Electrochemical impedance measurements on the solar cells fabricated using free base H₂TFP and the metal complex (ZnTFP) were carried out to understand charge transfer and energetics of charge transport and recombination. The impedance measurements were carried out at frequencies between 0 and 100 KHz. **Figure 11** shows the Nyquist plots (a) and Bode plots (b) of H₂TFP and ZnTFP,

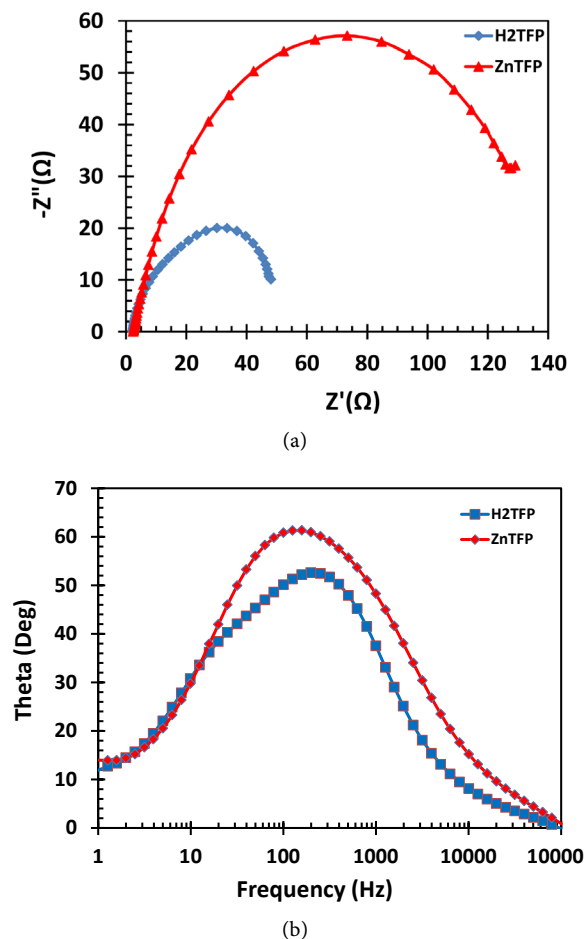


Figure 11. Impedance studies of the fabricated devices: (a) Nyquist plot of the dye sensitized solar cells fabricated using H₂TFP (blue) and ZnTFP (blue); (b) Bode plot of dye sensitized solar cells fabricated using H₂TFP (blue) and ZnTFP (red).

respectively. The arc in the high frequency region is usually associated with the charge transfer resistance at the interface between the redox couple/electrolyte and counter electrode whereas the arc in the low frequency region is ascribed to the resistance of the transport of the injected electrons within the TiO₂ film. The results seen here are consistent with the IV data. The impedance measurement also shows less overall resistance for the free porphyrin (50 Ω) compared with the zinc complex (130 Ω). The position of the low frequency peak of the Bode plot provides information on the lifetime of the photo induced electrons via the equation:

$$\tau = 1/(2\pi f) \quad (3)$$

where, f is the frequency of superimposed ac voltage. Thus, H₂TFP was found to have a longer lifetime than ZnTFP.

3.11. Density Functional Theory (DFT) Calculations

Density functional calculations were used to optimize the geometry of fluorenyl-porphyrin, H₂TFP, molecule using the software Spartan 16 from Wave function. All geometries were computed using the ωB97X-D density functional theory method. Geometry optimization was performed using 6-31G* basis set. These calculations were used to calculate the highest occupied molecular orbital (HOMO) and the lowest unoccupied molecular orbital (LUMO) energies of free base and metallic meso-tetrakis-2-(H9-fluorenyl) porphyrin coordinated to Zn (square planar complex).

Figure 12(a) and **Figure 12(b)**, show the Lewis and 3D structures of fluorene-porphyrin, respectively. Similarly, **Figure 12(c)** and **Figure 12(d)** show the

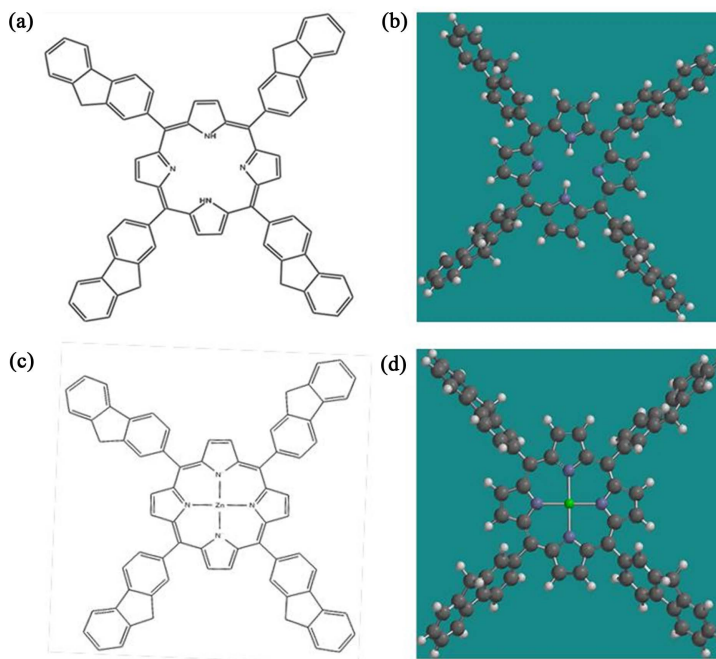


Figure 12. Lewis structure ((a), (c)) and 3D structure ((b), (d)) of free porphyrin ((a), (b)) and metallic porphyrin ((c), (d)).

Lewis and 3D structures of metallic meso-tetrakis-2-(H9-fluorenyl) porphyrin, respectively. The calculations gave a result for the HOMO as -6.29 eV and the result for the LUMO found to be -0.87 eV. Thus, the difference in the HOMO and LUMO which is the band gap was 5.42 eV. The calculations for the metallic compound gave a result for the HOMO as -6.36 eV and the result for the LUMO as -0.77 eV. The difference in the HOMO and LUMO which is the band gap was 5.59 eV. The HOMO and LUMO surfaces and orbital energy diagrams for the free base is displayed in **Figure 13(a)** and **Figure 13(b)** and that of metallic porphyrin are shown in **Figure 13(c)** and **Figure 13(d)**, respectively. The blue and red regions in all the figures represent the positive and negative values of these orbitals, respectively.

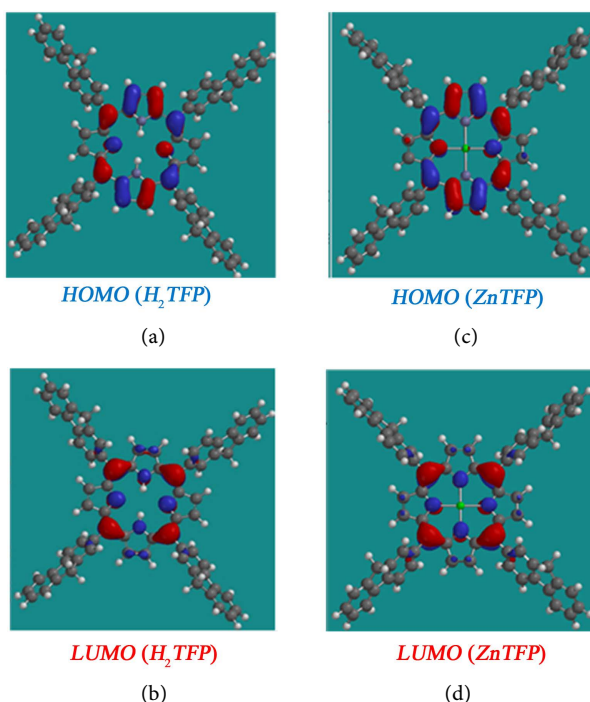


Figure 13. LUMO Energy diagram and surface ((a), (c)) and HOMO energy diagram and surface ((b), (d)) of the free Porphyrin ((a), (b)) and metallic porphyrin ((c) (d)).

3.12. Energy Diagram

In the presence of solar energy, porphyrin dye molecules (S) adsorbed on the TiO_2 film absorb photon and make a transition from the ground state or highest occupied molecular orbitals (HOMO) to the excited state or the lowest unoccupied molecular orbital (LUMO) state as displayed in **Figure 14**. The photoexcited dye species (S^*) injects an electron into the conduction band of TiO_2 electrode and becomes oxidized (S^+). The oxidized dye species subsequently accept an electron from the electrolyte (I^-) and the ground state of the dye (S) is restored. The injected electron is transported through the mesoporous TiO_2 film to the FTO layer and is conducted through an external circuit to a load where the work done is delivered as electrical energy. The electron from the external load diffuses to the cathode where it gets transferred to the electrolyte (I^{3-}).

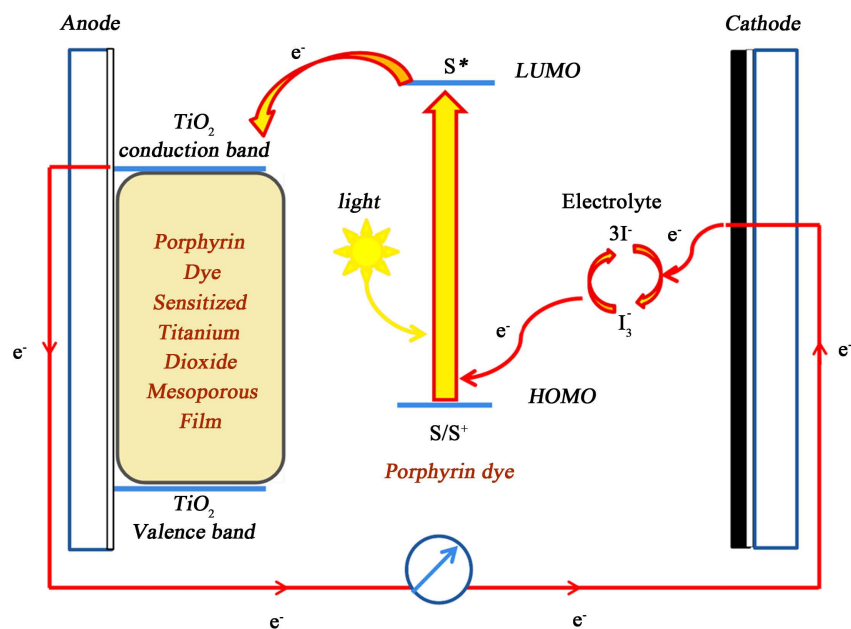


Figure 14. Energy diagram of porphyrin dye sensitized solar cell.

4. Conclusion

Two different porphyrin dyes were used to fabricate dye sensitized solar cells. The two porphyrin complexes comprised of a metal-free 5, 10, 15, 20-meso-tetrakis-(9H-2-fluorene-yl) porphyrin (H_2TFP) and its Zinc complex ($ZnTFP$). UV-Vis, Fluorescence, and Fourier Transformed Infrared measurements of the two dyes were carried out to evaluate their absorption, emission and binding characteristics. The Soret band of the dyes was almost the same while changes in the Q-band were observed. This observation was also confirmed in the fluorescence data where changes in peak intensity were due to Q-band. The surface morphology and elemental analysis of the porphyrin dye sensitized photoanodes were determined using Field Emission Scanning Electron Microscopy Imaging and Transmission Electron Microscopy Imaging. The nanocrystalline nature of the TiO_2 and their interaction with the dyes were clearly observed under the electron microscopes. Cyclic voltammetry studies, current-voltage characteristics and the electrochemical impedance spectroscopic studies were also carried out. Solar-to-electric energy efficiency of H_2TFP dye sensitized solar cell was higher (0.11%) than that of the zinc complex (0.08%). Thus the metal free porphyrin generated more power than the zinc complex under similar conditions. These efficiencies could be higher when anchoring groups are attached to the porphyrins. The free base H_2TFP chromophore was found to possess the best photosensitization effect among the two porphyrin dyes studied which has been attributed by the flexibility of the dye to interact.

Acknowledgements

The work was financially supported by the University of Maryland System (Wilson E. Elkins Professorship), Constellation, an Exelon Company (E2-Ener-

gy to Educate grant program) and Dept. of Education (SAFRA Title III Grant). The authors are also grateful to the Institution of Advancement, Coppin State University, for administrative help. The content is exclusively the responsibility of the authors and does not necessarily represent the official views of the funding agencies.

References

- [1] Wei, D. (2010) Dye Sensitized Solar Cells. *International Journal of Molecular Sciences*, **11**, 1103-1113. <https://doi.org/10.3390/ijms11031103>
- [2] Sugathan, V., John, E. and Sudhakar, K. (2015) Recent Improvements in Dye Sensitized Solar Cells: A Review. *Renewable and Sustainable Energy Reviews*, **52**, 54-64.
- [3] Gratzel, M. (2003) Dye-Sensitized Solar Cells. *Journal of Photochemistry and Photobiology C*, **4**, 145-153.
- [4] Grätzel, M. (2005) Solar Energy Conversion by Dye-Sensitized Photovoltaic Cells. *Inorganic Chemistry*, **44**, 6841-6851. <https://doi.org/10.1021/ic0508371>
- [5] O'Regan, B. and Gratzel, M. (1991) A Low-Cost, High-Efficiency Solar Cell Based on Dye-Sensitized Colloidal TiO₂ Films. *Nature*, **353**, 737-740. <https://doi.org/10.1038/353737a0>
- [6] Hug, H., Bader, M., Mair, P. and Glatzel, T. (2014) Biophotovoltaics: Natural Pigments in Dye-Sensitized Solar Cells. *Applied Energy*, **115**, 216-225.
- [7] Hao, S., Wu, J., Huang, Y. and Lin, J. (2006) Natural Dyes as Photosensitizers for Dye-Sensitized Solar Cell. *Solar Energy*, **80**, 209-214.
- [8] Amadi, L., Jenny, S.S., Ahmed, A., Brown, N., Yadav, S., Brown, D., Ghann, W., Gayrama, A., Jiru, M. and Uddin, J. (2015) Creation of Natural Dye Sensitized Solar Cell by Using Nanostructured Titanium Oxide. *Nanoscience and Nanoengineering*, **3**, 25-35. <https://doi.org/10.13189/nn.2015.030301>
- [9] Ghann, W., Kang, H., Sheikh, T., Yadav, S., Chavez-Gil, T., Nesbitt, F. and Uddin, J. (2017) Fabrication, Optimization and Characterization of Natural Dye Sensitized Solar Cell. *Scientific Reports*, **7**, Article No. 41470. <https://doi.org/10.1038/srep41470>
- [10] Ludin, N.A., Al-Alwani Mahmoud, A.M., Bakar Mohamad, A., Kadhum, A.A.H., Sopian, K. and Abdul Karim, N.S. (2014) Review on the Development of Natural Dye Photosensitizer for Dye-Sensitized Solar Cells. *Renewable and Sustainable Energy Reviews*, **31**, 386-396.
- [11] Yadav, S., Jenny, S.S., Ahmed, A., Amadi, L., Nesbitt, F., Ward, A.W.G., Brown, D., Uddin, J. and Uddin, N. (2015) Natural Light-Harvesting Sensitizers for Dye Sensitized Solar Cell. *Energy and Environmental Engineering*, **3**, 94-99. <https://doi.org/10.13189/eee.2015.030403>
- [12] Shalini, S., Balasundara Prabhu, R., Prasanna, S., Mallick, T.K. and Senthilarasu, S. (2015) Review on Natural Dye Sensitized Solar Cells: Operation, Materials and Methods. *Renewable and Sustainable Energy Reviews*, **51**, 1306-1325.
- [13] Wu, W., Guo, F., Li, J., He, J. and Hua, J. (2010) New Fluoranthene-Based Cyanine Dye for Dye-Sensitized Solar Cells. *Synthetic Metals*, **160**, 1008-1014.
- [14] Akhtaruzzaman, M., Islam, A., Yang, F., Asao, N., Kwon, E., Singh, S.P., Han, L. and Yamamoto, Y. (2011) A Novel Metal-Free Panchromatic TiO₂ Sensitizer Based on a Phenylenevinylene-Conjugated Unit and an Indoline Derivative for Highly Efficient Dye-Sensitized Solar Cells. *Chemical Communications*, **47**, 12400-12402. <https://doi.org/10.1039/c1cc15580f>

- [15] Chen, C.Y., Wang, M., Li, J.Y., Pootrakulchote, N., Alibabaei, L., Ngoc-Le, C.H., Decoppet, J.D., Tsai, J.H., Grätzel, C., Wu, C.G., Zakeeruddin, S.M. and Grätzel, M. (2009) Highly Efficient Light-Harvesting Ruthenium Sensitizer for Thin-Film Dye-Sensitized Solar Cells. *ACS Nano*, **3**, 3103-3109. <https://doi.org/10.1021/nn900756s>
- [16] Klein, C., Nazeeruddin, M.K., Censo, D.D., Liska, P. and Grätzel, M. (2004) Amphiphilic Ruthenium Sensitizers and Their Applications in Dye-Sensitized Solar Cells. *Inorganic Chemistry*, **43**, 4216-4226. <https://doi.org/10.1021/ic049906m>
- [17] Bhaumik, J., Weissleder, R. and McCarthy, J.R. (2009) Synthesis and Photophysical Properties of Sulfonamidophenyl Porphyrins as Models for Activatable Photosensitizers. *The Journal of Organic Chemistry*, **74**, 5894-5901. <https://doi.org/10.1021/jo900832y>
- [18] Daphnomili, D., Landrou, G., Prakash Singh, S., Thomas, A., Yesudas, K., Bhanuprakash, K., Sharma, G.D. and Coutsolelos, A.G. (2012) Photophysical, Electrochemical and Photovoltaic Properties of Dye Sensitized Solar Cells Using a Series of Pyridyl Functionalized Porphyrin Dyes. *RSC Advances*, **2**, 12899-12908. <https://doi.org/10.1039/c2ra22129b>
- [19] Daphnomili, D., Sharma, G.D., Biswas, S., Justin Thomas, K.R. and Coutsolelos, A.G. (2013) A New Porphyrin Bearing a Pyridinylethynyl Group as Sensitizer for Dye Sensitized Solar Cells. *Journal of Photochemistry Photobiology A: Chemistry*, **253**, 88-96.
- [20] Gou, F., Jiang, X., Li, B., Jing, H. and Zhu, Z. (2013) Salicylic Acid as a Tridentate Anchoring Group for *azo*-Bridged Zinc Porphyrin in Dye-Sensitized Solar Cells. *ACS Applied Materials & Interfaces*, **5**, 12631-12637. <https://doi.org/10.1021/am403987b>
- [21] Hart, A.S., Chandra, B.K.C., Gobeze, H.B., Sequeira, L.R. and D'Souza, F. (2013) Porphyrin-Sensitized Solar Cells: Effect of Carboxyl Anchor Group Orientation on the Cell Performance. *ACS Applied Materials & Interfaces*, **5**, 5314-5323. <https://doi.org/10.1021/am401201q>
- [22] He, H., Gurung, A. and Si, L. (2012) 8-Hydroxylquinoline as a Strong Alternative Anchoring Group for Porphyrin-Sensitized Solar Cells. *Chemical Communications*, **48**, 5910-5912. <https://doi.org/10.1039/c2cc31440a>
- [23] Higashino, T. and Imahori, H. (2015) Porphyrins as Excellent Dyes for Dye-Sensitized Solar Cells: Recent Developments and Insights. *Dalton Transactions*, **44**, 448-463. <https://doi.org/10.1039/C4DT02756F>
- [24] Lan, C.M., Wu, H.P., Pan, T.Y., Chang, C.W., Chao, W.S., Chen, C.T., Wang, C.L., Lin, C.Y. and Diao, E.W.G. (2012) Enhanced Photovoltaic Performance with Co-Sensitization of Porphyrin and an Organic Dye in Dye-Sensitized Solar Cells. *Energy & Environmental Science*, **5**, 6460-6464. <https://doi.org/10.1039/c2ee21104a>
- [25] Mai, C.-L., Moehl, T., Hsieh, C.-H., Decoppet, J.-D., Zakeeruddin, S.M., Grätzel, M. and Yeh, C.-Y. (2015) Porphyrin Sensitizers Bearing a Pyridine-Type Anchoring Group for Dye-Sensitized Solar Cells. *ACS Applied Materials & Interfaces*, **7**, 14975-14982. <https://doi.org/10.1021/acsami.5b03783>
- [26] Mathew, S., Yella, A., Gao, P., Humphry-Baker, R., Curchod, B.F.E., Ashari-Astani, N., Tavernelli, I., Rothlisberger, U., Nazeeruddin, M.K. and Grätzel, M. (2014) Dye-Sensitized Solar Cells with 13% Efficiency Achieved through the Molecular Engineering of Porphyrin Sensitizers. *Nature Chemistry*, **6**, 242-247. <https://doi.org/10.1038/nchem.1861>
- [27] Armarego, W.L. and Chai, C. (2009) Purification of Laboratory Chemicals. 6th Edition, Butterworth-Heinemann, Elsevier, UK.
- [28] Mamardashvili, N.Zh. and Golubchikov, O.A. (2001) Spectral Properties of Porphyrin

- rins and Their Precursors and Derivatives. *Russian Chemical Reviews*, **70**, 577-606. <https://doi.org/10.1070/RC2001v070n07ABEH000661>
- [29] Walker, F.A., Balke, V.L. and McDermott, G.A. (1982) Electronic Effects in Transition-Metal Porphyrins. 4. Effect of Unsymmetrical Phenyl Substitution on the NMR Spectra of a Series of Metal-Free and Zinc Tetraphenylporphyrins. *Inorganic Chemistry*, **21**, 3342-3348.
- [30] Kevin, M., Smith, K.M., Abraham, R.J. and Pearson, H. (1982) The NMR Spectra of Porphyrins—19. *Tetrahedron*, **38**, 2441-2449.
- [31] Drouet, S., Merhi, A., Argouarch, G., Paul, F., Mongin, O., Blanchard-Desce, M. and Paul-Roth, C.O. (2012) Synthesis of New Luminescent Supramolecular Assemblies from Fluorenyl Porphyrins and Polypyridyl Isocyanurate-Based Spacers. *Tetrahedron*, **68**, 98-105.
- [32] Gouterman, M. (1961) Spectra of Porphyrins. *Journal of Molecular Spectroscopy*, **6**, 138-163.
- [33] Spellane, P.J., Gouterman, M., Antipas, A., Kim, S. and Liu, Y.C. (1980) Porphyrins. 40. Electronic Spectra and Four-Orbital Energies of Free-Base, Zinc, Copper, and Palladium Tetrakis(Perfluorophenyl)Porphyrins. *Inorganic Chemistry*, **19**, 386-391. <https://doi.org/10.1021/ic50204a021>
- [34] Gouterman, M. (1979) The Porphyrins. Vol. III, Academic Press, New York.
- [35] Liu, W., Shi, Y.-H., Wang, Y.-J., Shi, T.-S. and Zhang, W.-J. (2003) Synthesis of Tetra(4-n-Lauryloxyphenyl)Porphyrin Complexes and Its Liquid Crystalline Characterization. *Chemical Journal of Chinese Universities*, **24**, 200-204.
- [36] Michaelian, K.H., Wen, Q., Billingham, B.E., Shaw, J.M. and Lastovka, V. (2012) Far- and Mid-Infrared Photoacoustic Spectra of Tetracene, Pentacene, Perylene and Pyrene. *Vibrational Spectroscopy*, **58**, 50-56.
- [37] Boersma, C., Mattioda, A.L., Bauschlicher Jr., C.W., Peeters, E., Tielens, A.G.G.M. and Allamandola, L.J. (2009) The 5.25 and 5.7 μm Astronomical Polycyclic Aromatic Hydrocarbon Emission Features. *The Astrophysical Journal*, **690**, 1208. <https://doi.org/10.1088/0004-637X/690/2/1208>
- [38] Joblin, C., d'Hendecourt, L., Léger, A. and Défourneau, D. (1994) Infrared Spectroscopy of Gas-Phase PAH Molecules. *Astronomy and Astrophysics*, **281**, 923-936.
- [39] Szczepanski, J. and Vala, M. (1993) Infrared Frequencies and Intensities for Astrophysically Important Polycyclic Aromatic Hydrocarbon Cations. *Astrophysical Journal*, **414**, 646-655. <https://doi.org/10.1086/173110>
- [40] Gritzner, G. and Kuta, J. (1984) Recommendations on Reporting Electrode Potentials in Nonaqueous Solvents. *Pure & Applied Chemistry*, **56**, 461-466. <https://doi.org/10.1351/pac198456040461>
- [41] Rault-Berthelot, J., Paul-Roth, C., Poriel, C., Juillard, S., Ballut, S., Drouet, S. and Simonneaux, G. (2008) Comparative Behaviour of the Anodic Oxidation of Mono-, Di- and Tetra-Arylporphyrins: Towards New Electroactive Materials with Variable Bandgaps. *Journal of Electroanalytical Chemistry*, **623**, 204-214.
- [42] Felton, R.H. and Linschitz, H. (1966) Polarographic Reduction of Porphyrins and Electron Spin Resonance of Porphyrin Anions. *Journal of the American Chemical Society*, **88**, 1113-1116. <https://doi.org/10.1021/ja00958a004>
- [43] Kadish, K.M., Sazou, D., Liu, Y.M., Saoiabi, A., Ferhat, M. and Guillard, R. (1988) Electrochemical and Spectral Characterization of the Monomer-Dimer Equilibrium Involving (Meso-tetrakis(1-methylpyridinium-4-yl)porphinato)nickel(II) in Dimethylformamide. *Inorganic Chemistry*, **27**, 686-690. <https://doi.org/10.1021/ic00277a023>

- [44] Engelmann, F.M., Losco, P., Winnischofer, H., Araki, K. and Toma, H.E. (2002) Synthesis, Electrochemistry, Spectroscopy and Photophysical Properties of a Series of Meso-Phenylpyridylporphyrins with One to Four Pyridyl Rings Coordinated to [Ru(bipy)₂Cl]⁺ Groups. *Journal of Porphyrins and Phthalocyanines*, **6**, 33-42. <https://doi.org/10.1142/S1088424602000063>
- [45] Paul-Roth, C.O. and Simonneaux, G. (2006) Porphyrins with Fluorenyl and Fluorenone Pendant arms. *Tetrahedron Letters*, **47**, 3275-3278.
- [46] Paul-Roth, C., Rault-Berthelot, J., Simonneaux, G., Letessier, J. and Bergamini, J.-F. (2007) Selective Anodic Preparation of 1D or 2D Electroactive Deposits from 5, 15-Bis-(9H-fluoren-2-yl)-10,20-Diphenyl Porphyrins. *Journal of Electroanalytical Chemistry*, **606**, 103-116.
- [47] Paul-Roth, C.O. and Simonneaux, G. (2006) Porphyrins with Fluorenyl and Fluorenone Pendant Arms as Red-Light-Emitting Devices. *Comptes Rendus Chimie*, **9**, 1277-1286.
- [48] Reed, R.A., Purrello, R., Prendergast, K. and Spiro, T.G. (1991) Resonance Raman Characterization of the Radical Anion and Triplet States of Zinc Tetraphenylporphyrine. *The Journal of Physical Chemistry*, **95**, 9720-9727. <https://doi.org/10.1021/j100177a024>
- [49] Li, B., Li, J., Fu, Y. and Bo, Z. (2004) Porphyrins with Four Monodisperse Oligofluorene Arms as Efficient Red Light-Emitting Materials. *Journal of the American Chemical Society*, **126**, 3430-3431. <https://doi.org/10.1021/ja039832y>
- [50] Lever, A.B.P. (1990) Electrochemical Parametrization of Metal Complex Redox Potentials, Using the Ruthenium(III)/Ruthenium(II) Couple to Generate a Ligand Electrochemical Series. *Inorganic Chemistry*, **29**, 1271-1285. <https://doi.org/10.1021/ic00331a030>



Scientific Research Publishing

Submit or recommend next manuscript to SCIRP and we will provide best service for you:

Accepting pre-submission inquiries through Email, Facebook, LinkedIn, Twitter, etc.

A wide selection of journals (inclusive of 9 subjects, more than 200 journals)

Providing 24-hour high-quality service

User-friendly online submission system

Fair and swift peer-review system

Efficient typesetting and proofreading procedure

Display of the result of downloads and visits, as well as the number of cited articles

Maximum dissemination of your research work

Submit your manuscript at: <http://papersubmission.scirp.org/>

Or contact ampc@scirp.org